2021 43rd Annual International Conference of the
IEEE Engineering in Medicine & Biology Society (EMBC)
Oct 31 - Nov 4, 2021. Virtual Conference

Analysis of Human Head Motion and Robotic Compensation for PET Imaging Studies

Yangzhe Liu[1], Ti Wu[2,3], Iulian I. Iordachita[1], Caroline Paquette[4], and Peter Kazanzides[2]

***Abstract*— Functional medical imaging systems can provide insights into brain activity during various tasks, but most current imaging systems are bulky devices that are not compatible with many human movements. Our motivating application is to perform Positron Emission Tomography (PET) imaging of subjects during sitting, upright standing and locomotion studies on a treadmill. The proposed long-term solution is to construct a robotic system that can support an imaging system surrounding the subject's head, and then move the system to accommodate natural motion. This paper presents the first steps toward this approach, which are to analyze human head motion, determine initial design parameters for the robotic system, and verify the concept in simulation.**

I. Introduction

Positron Emission Tomography (PET) is a prime imaging modality for neuroscience research because it provides functional imaging of brain activity. Conventional PET scanners are large pieces of equipment optimized for scanning the whole body and require subjects to lie still on a scanning bed. This restriction led to the development of a wearable PET imaging system, called Helmet_PET [1], [2], a concept that has since been investigated by others. While a wearable PET imager is ideal for avoiding interference with human motion, the resulting weight limitation reduces sensitivity, thereby requiring higher radiotracer dose. A recent review by Majewski [3], inventor of Helmet_PET, indicated that active mechanical support, through robotics (e.g., Figs. 27-28 in [3]), could enable use of the heavier detectors (15-20 kg) that would provide higher sensitivity and therefore reduced dose.

Development of a robotic system to support PET imaging of the brain during motion requires an understanding of the motion parameters that would serve as design input for the robotic system. In this paper, we consider neuroscience research in human locomotion, performed on a treadmill, and therefore characterize head motion during walking. We assume a robotic system such as the one shown in Fig. 1, where the subject is walking on a treadmill, with the robotic system supporting the PET imaging ring around the subject's head. The subject is wearing a helmet that provides both safety and facilitates the real-time measurement of head motion. For example, this motion can be measured by cameras on the imaging ring tracking markers on the helmet, or by multiple string encoders connected between the imaging ring and helmet.

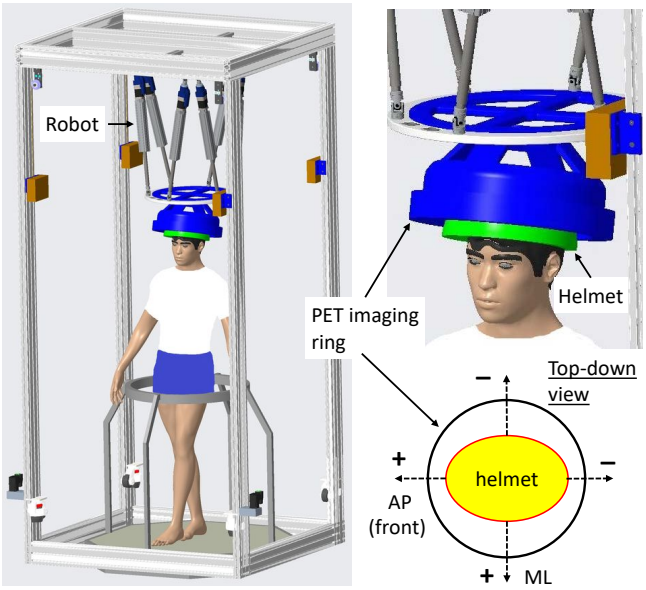

Fig. 1. Concept for robot-assisted PET imaging. Left: Subject walks on treadmill, while robotic system measures head motion and moves imaging ring to avoid collision; Top-right: Closeup showing PET imaging ring and helmet. Bottom-right: Top-down view showing AP and ML directions.

Once the head position is measured, the robot system will move the PET imaging ring to keep the head as close as possible to the ring center. This is primarily to avoid collision between the imaging ring and helmet because, given the measured head position, the PET image reconstruction software will correct for displacements of the head with respect to the imaging ring. This displacement of the head is unavoidable due to the latency, or delay, of the robot system, which is the time elapsed between receiving an action command and perceiving its consequences in the real environment [4]. Most robots and electronic devices exhibit several milliseconds delay, which causes a discrepancy between the robot end-effector position and the target location.

The contributions of this paper are: (1) an analysis of human head motion during walking, (2) simulation of robotic compensation for this head motion, assuming a simple delay model for the robot, and (3) an exploration of the design space considering different robot delays and imaging ring diameters.

[1] Dept. of Mechanical Engineering, Johns Hopkins University, Baltimore USA, [yliu335, iordachita]@jhu.edu
[2] Dept. of Computer Science, Johns Hopkins University, Baltimore USA, [twu51, pkaz]@jhu.edu
[3] School of Instrument Science and Engineering, Southeast University, Nanjing, China, wuti@seu.edu.cn
[4] Dept. of Kinesiology and Physical Education, McGill University, Montreal, Canada, caroline.paquette@mcgill.ca

II. METHODS

A. Data Acquisition

1) Motion Capture Data: Full-body motion data from sixteen healthy control subjects (mean age: 62 years, range: 43-80 years), collected in a previous study [5] [6], were analyzed. The subjects were recorded during overground walking in a straight line, captured by a motion capture system (Motion Analysis, Santa Rosa, CA). Retroreflective markers were positioned on 45 body landmarks and their 3D positions, with respect to a fixed world frame, were collected at a sampling frequency of 60 Hz. The world frame was defined such that the direction of walking was primarily in the +X direction, with the +Y direction to the left and the +Z direction upward. These are illustrated in Fig. 1, with the X axis represented by AP (Anterior-Posterior), the Y axis by ML (Medial-Lateral) and the Z axis by UD (Up-Down).

2) Inertial Measurement Unit (IMU) Data: We obtained acceleration data from eight healthy participants (mean age: 22 years, range: 18-28 years), collected in a previous study [7] that used seven IMUs (APDM, Portland, OR) placed on subjects walking on a treadmill, sampled at 128 Hz.

B. Motion Capture Data Analysis

1) Emulating Treadmill Walking: We used one head marker (LEYE, left side of the front of the head) to indicate head motion. Because we are interested in head motion during treadmill walking, we subtracted the motion due to overground walking, which we estimated by fitting a line to the data from one body marker at C7 (cervical vertebra). This essentially models the overground walking as a constant velocity. We then use equation (1) to calculate the head motion in the AP and ML directions. It was necessary to correct the ML measurements because the world frame was not perfectly aligned with the direction of walking, which led to apparent drift. The UD direction was not affected and therefore it was not necessary to subtract the best-fit line.

$$P_{head} = P_{LEYE} - P_{c7BestFit} \tag{1}$$

We then shifted all the P_{head} to zero mean, since we are interested in head motion relative to a nominal center position.

2) Outlier Removal: Outliers are present in the beginning and end of each data set, corresponding to the times before and after the subject performed the overground walking. We identified the start and end of the actual overground walking as follows, where N is the number of position measurements in each sample:

1) Identify the maximum positions (in x, y, z) in the middle 60% of the data set, given by $0.2N - 0.8N$.
2) Start at sample $0.2N$ and search toward the beginning of the data until a position greater than 1.5 times the maximum is found. Remove all data up to and including this sample.
3) Start at sample $0.6N$ and search toward the end of the data until a position greater than 1.5 times the maximum is found. Remove all data from this sample to the end.

3) Estimation of Velocity and Acceleration: The velocity, V_t, and acceleration, A_t, were calculated using the central difference, equation (2), where dt is the sampling period.

$$V_t = \frac{P_{t+1} - P_{t-1}}{2dt} \quad A_t = \frac{V_{t+1} - V_{t-1}}{2dt} \tag{2}$$

C. IMU Data Processing

We used the acceleration data from an IMU attached to the forehead, with the +Z direction forward, the +X direction downward, and the +Y direction toward the left. We rotated these readings to align with the world coordinate system defined for the motion capture data.

Because an accelerometer measures both body acceleration and acceleration due to gravity, we subtracted the mean acceleration in each direction to eliminate the effect of gravity as well as any measurement bias. Even though gravity should only affect the measurement in the downward direction, we anticipated non-zero mean accelerations in other directions due to imperfect alignment of the IMU.

D. Comparison of Motion Capture and IMU Data

The purpose of the IMU data is to validate the relevance of the motion capture data for treadmill motion, considering that the latter was collected during overground walking. We compare the accelerometer measurement (after subtracting gravity) to the acceleration estimated from the position data, both statistically (e.g., standard deviation, maximum) and via a Fourier analysis using the Matlab Fast Fourier Transform.

E. Preliminary Robot Design

A recent study [8] of anthropometric measurements shows that 97.5% of humans have head lengths up to 213 mm in the AP (anterior-posterior) direction and widths up to 165 mm in the ML (medio-lateral) direction. Allowing a constant helmet thickness of 25 mm (1 inch) leads to a helmet of dimension 263 mm x 215 mm. With an imaging ring diameter of 300 mm, this leads to a radial clearance of 18 mm in the AP direction and 42 mm in the ML direction.

F. Robot Control Simulation

One simple model for a robot system is a low-pass filter, which attenuates higher-frequency signals and also imposes a delay (phase shift). Our analysis (Section III-B) indicates that the head motion is primarily within the typical robot bandwidth (1-20 Hz), so we can adopt an even simpler model of just a time delay. Specifically, we provide the processed head position data, described above, as the commanded position to the simulated robot and use the delayed commanded position as the actual robot position. We evaluate with different delays to provide guidance into the requirements and design of the robot system. Our range of delays is consistent with values reported in the literature. For example, the actuation delay for a UR5 robot arm (Universal Robots, Odense, Denmark) is around 70 ms [9].

Subtracting the delayed output from the input indicates the displacement of the head from the center; to avoid collision with the imaging ring, this displacement should be smaller than the clearance between the helmet and imaging ring.

III. Results

A. Analysis of Human Head Motion

After processing the motion capture data and eliminating outliers, we calculated the velocity and acceleration using equation (2). Figure 2 shows a sample plot of motion results for one human subject. We then plotted histograms of the acceleration estimated from the motion capture data and from the IMU, as shown in Fig. 3, to verify that a normal distribution would be a reasonable model. As mentioned previously, the IMU data in each direction was shifted to zero mean; the original means were 2.82 m/s^2, 0.25 m/s^2 and -9 m/s^2 in the AP, ML and UD directions, respectively. The norm of the mean accelerations is 9.43 m/s^2, which is consistent with gravity (9.81 m/s^2) and possibly some uncompensated bias.

Table I shows the statistics of the motion data for all 16 subjects in the motion capture experiment and all 8 subjects in the IMU experiment.

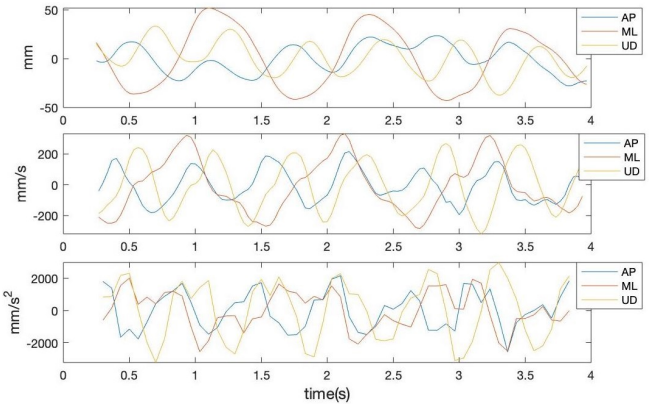

Fig. 2. Sample plot of relative head position/velocity/acceleration.

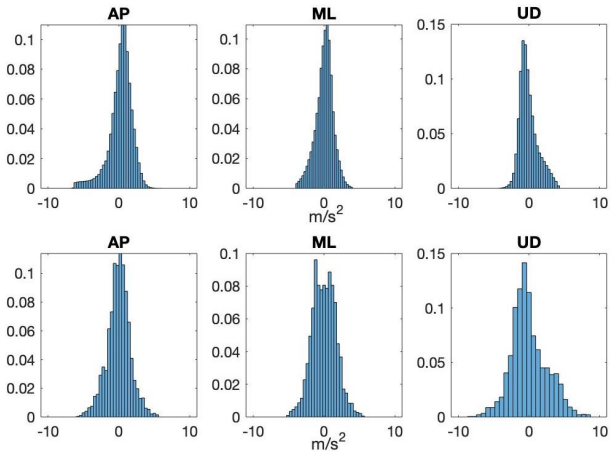

Fig. 3. Histograms for IMU data (top) and Motion Capture data (bottom); horizontal units are m/s^2,vertical axes were normalized to relative probability.

B. Comparison of Motion Capture and IMU Data

The maximums and standard deviations of the accelerations derived from the motion capture data and from the IMU can be compared in Table I. The values in the AP and ML directions are similar; in the UD direction, the values for the motion capture data (overground walking) are approximately twice as large as those for the IMU data (treadmill walking).

TABLE I

Motion data for all subjects; values given are range, standard deviation (SD) and maximum.

Motion Capture (N=16)	**AP**	**ML**	**UD**
Pos. Range, mm	67	82	43
Pos. SD, mm	18.8	22	11.3
Vel. Max, mm/s	207	258	228
Vel. SD, mm/s	68.9	111.4	111.6
Acc. Max, mm/s^2	5411	5348	8116
Acc. SD, mm/s^2	1633	1683	2541
IMU (N=8)	**AP**	**ML**	**UD**
Acc. Max, mm/s^2	6578	4004	4200
Acc. SD, mm/s^2	1676	1246	1316

In addition, we applied Fast Fourier Transforms on the measured head motion and on the IMU acceleration data, as shown in Fig. 4. These plots demonstrate that the motion capture data (processed to remove the effect of overground walking) and the IMU treadmill data share similar spectral properties, with most frequencies below 5 Hz.

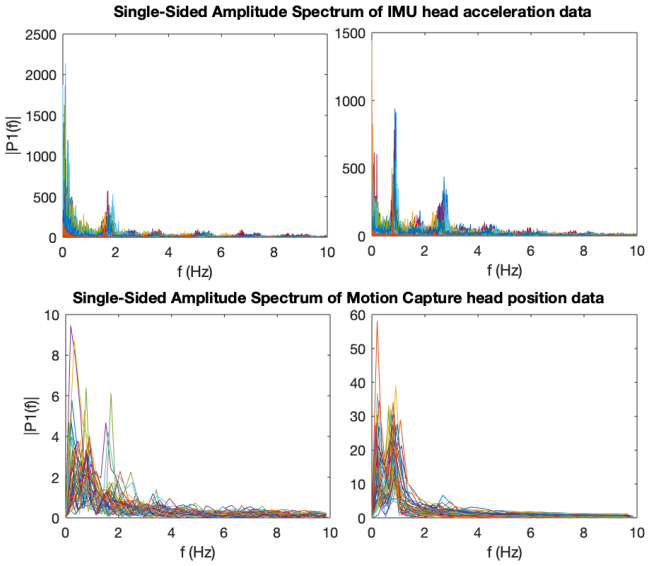

Fig. 4. Fourier transform of IMU acceleration and Motion Capture position; plot was truncated at 10 Hz as the amplitudes are insignificant above 10 Hz.

C. Robot Control Simulation

We simulated the effect of using a robot to compensate for the measured head motion, where the robot was modeled as a time delay (as in a low pass filter). The motion capture sampling frequency was 60 Hz (period of 16.67 ms), so we considered time delays that were multiples of the sampling period, from 16.67 ms to 166.67 ms. The uncompensated (residual) head motion was given by the difference between the measured head position and the robot position (i.e., delayed head position). Figure 5 shows the result, in the AP and ML directions, for a delay of 66.67 ms (4 samples). The horizontal dashed lines indicate the clearances based on the preliminary design from Section II-E (18 mm and

42 mm in the AP and ML directions). Table II shows the three-sigma uncompensated motion in all three directions (i.e., where 99.7% of the motions fall within this limit) for all 16 participants.

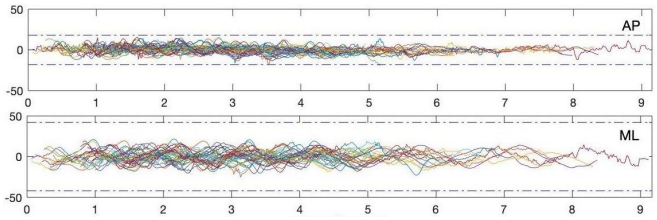

Fig. 5. Uncompensated head motion in mm, with robot delay of 66.67 ms, using measured data from all 16 subjects; horizontal axis is time in seconds.

TABLE II
THREE-SIGMA UNCOMPENSATED HEAD MOTION UNDER DIFFERENT ROBOT DELAYS

Delay, ms	***AP,*** mm	***ML,*** mm	***UD,*** mm
16.67	4.2	5.8	5.6
33.33	6.8	11.0	10.8
50.00	9.7	16.3	16.0
66.67	12.5	21.6	21.0
83.33	15.3	26.8	25.8
100.00	18.0	32.0	30.4
116.67	20.5	37.0	34.7
133.33	23.0	42.0	38.7
150.00	25.3	46.8	42.3
166.67	27.6	51.6	45.7

D. Design Exploration

Figure 6 shows the required clearances, for the AP and ML directions, between the helmet and imaging ring as a function of the robot delay time, where the clearance is based on the maximum (solid lines) or three-sigma (dashed lines) uncompensated head motion.

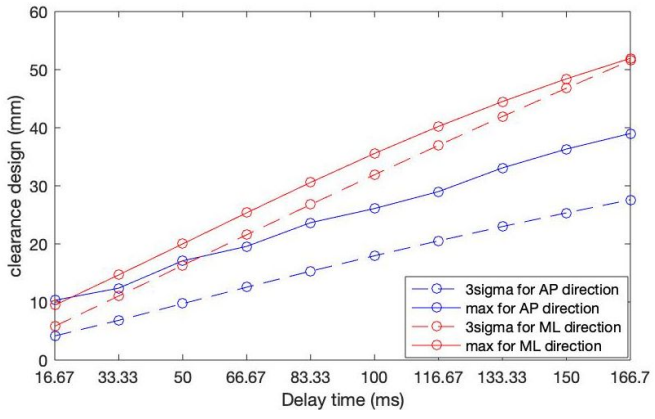

Fig. 6. Design parameters based on maximum (solid lines) and three-sigma (dashed lines) uncompensated head motions.

IV. Discussion and Conclusions

In this study, we analyzed recorded human motion to enable the design of a robotic system that can support a heavy imaging ring around a human head, and move that ring to accommodate normal head motions during treadmill walking. The primary data consisted of 3D positions captured during overground walking experiments, adjusted to emulate treadmill walking. The velocities and accelerations were computed, and the accelerations were compared to a secondary data set of accelerations provided by an inertial measurement unit (IMU) during treadmill walking. The maximums and standard deviations of the accelerations in the AP and ML directions were similar, as were the frequency domain characteristics. The values in the UD direction showed larger differences, but are less critical for the design because the imaging ring diameter does not restrict motion in this direction. Therefore, we conclude that the processed motion capture data sufficiently represents head motion during treadmill walking to support the design of the robotic system. Limitations of this study are that the overground walking and treadmill walking data were obtained from different subject populations, and both consisted of healthy volunteers without neurological impairment.

We then simulated robotic compensation for head motion by modeling the robot as a time delay. The results indicate that the preliminary design of a 300 mm diameter imaging ring, with clearances of 18 mm and 42 mm in the AP and ML directions, is sufficient for robot delays up to about 100 ms. For larger delays, it would be necessary to increase the imaging ring diameter to avoid collisions. Our future work includes evaluation with a physical robot, where the dynamic performance would be more complex than a fixed time delay.

Acknowledgments

We thank Stan Majewski for initiating the investigation of robotic compensation for head motion during PET imaging, and for subsequent discussions with Emad Boctor, Arman Rahmim, Jinyi Qi, Youngho Seo, Jean-Paul Soucy and others.

References

[1] S. Majewski and J. Proffitt, "Compact and mobile high resolution PET brain imager," 2011, US Patent 7,884,331.

[2] S. Majewski, J. Proffitt, J. Brefczynski-Lewis, A. Stolin, A. Weisenberger, W. Xi, and R. Wojcik, "HelmetPET: A silicon photomultiplier based wearable brain imager," in *IEEE Nuclear Science Symposium and Medical Imaging Conference Record*, Valencia, Spain, Oct. 2011, pp. 4030–4034.

[3] S. Majewski, "The path to the "ideal" brain PET imager: The race is on, the role for TOF PET," *Il Nuovo Cimento C*, vol. 43, no. 1, pp. 1–35, 2020.

[4] S. Behnke, A. Egorova, A. Gloye, R. Rojas, and M. Simon, "Predicting away robot control latency," in *RoboCup 2003: Robot Soccer World Cup VII*, 2004, pp. 712–719.

[5] S. D. Israeli-Korn, A. Barliya, C. Paquette, E. Franzén, R. Inzelberg, F. B. Horak, and T. Flash, "Intersegmental coordination patterns are differently affected in Parkinson's disease and cerebellar ataxia," *Journal of Neurophysiology*, vol. 121, no. 2, pp. 672–689, 2019.

[6] C. Paquette, E. Franzén, G. M. Jones, and F. B. Horak, "Walking in circles: navigation deficits from Parkinson's disease but not from cerebellar ataxia," *Neuroscience*, vol. 190, pp. 177–183, 2011.

[7] D. C. Hinton, A. Thiel, J.-P. Soucy, L. Bouyer, and C. Paquette, "Adjusting gait step-by-step: Brain activation during split-belt treadmill walking," *Neuroimage*, vol. 202, p. 116095, 2019.

[8] Y. Rodrigues, "Anthropometric analysis of human head for designing ballistic helmets," *Procedia Manufacturing*, vol. 3, pp. 5475–5481, 2015.

[9] T. Andersen, *Optimizing the Universal Robots ROS driver.* Technical University of Denmark, Department of Electrical Engineering, 2015.